# Freak waves under typhoon conditions

Nobuhito Mori[1]

Received 1 December 2011; revised 10 February 2012; accepted 28 February 2012; published 17 April 2012.

[1] Benjamin-Feir Index (BFI) and directional spread are measures of nonlinear four-wave interactions and resultant indices of possible conditions for freak waves. Temporal-spatial distributions of BFI and directional spread are examined with numerical simulations of a spectral wave model using typhoon conditions. The spatial distributions of wave characteristics such as significant wave height, wave period, BFI and directional spread are different from each other around the eye of the typhoon. BFI is significantly large in the fourth quadrant of the typhoon, while waves are steep and have narrow frequencies and directional spectra. Freak waves resulting from nonlinear four-wave-wave interactions have a greater potential of occurring in the fourth quadrant of the typhoon than in the other quadrants. Furthermore, crossing sea states from two-wind-wave systems can be observed behind the eye of the typhoon. The crossing, two-wind systems are also dangerous sea states, although as observed, they are closer to linear wave conditions. Finally, the characteristics of possible freak wave conditions during typhoons are verified with field data.

**Citation:** Mori, N. (2012), Freak waves under typhoon conditions, *J. Geophys. Res.*, *117*, C00J07, doi:10.1029/2011JC007788.

## 1. Introduction

[2] Freak waves are sometimes featured with a single, steep crest causing severe damage to offshore structures and ships. Over the last decade freak waves have become an important topic in engineering and science. Freak wave studies started in the late 1980s [*Dean*, 1990] and high-order nonlinear effects of freak waves were discussed in the early 1990s at several engineering conferences [*Yasuda et al.*, 1992]. Evidence of freak wave generation in the ocean was reported from field observations in the North Sea [*Guedes Soares et al.*, 2003], the Sea of Japan [*Yasuda and Mori*, 1997] and the Gulf of Mexico [*Guedes Soares et al.*, 2004]. Due to the many research efforts, the occurrence of freak waves, their mechanisms, and their detailed dynamic properties are now becoming more clear [*Trulsen and Dysthe*, 1997; *Lavrenov*, 1998; *Osborne et al.*, 2000; *Onorato et al.*, 2001; *Mori et al.*, 2002]. The state of the art on freak waves was well summarized at the last *Rogue Wave Conferences*, held in 2008, and in a review by *Dysthe et al.* [2008] and *Kharif et al.* [2008].

[3] Freak wave generation is sometimes discussed in the context of nonlinear instability of deep water waves given the steep nature of the wave profile itself. *Janssen* [2003] found that the ratio between steepness (a measure of nonlinearity) and spectral bandwidth (a measure of dispersion) is an important parameter to determine the probability of finding a large wave. After *Janssen* [2003], this ratio between nonlinearity and dispersion was named the Benjamin-Feir Index (BFI); its relation to kurtosis, fourth-order moment of surface elevation, has been found by *Janssen* [2003] in the limit of large times and for narrow-banded spectra neglecting directional dispersion. Here we define the Benjamin-Feir Index as

$$BFI = \frac{\sqrt{2}\epsilon}{\delta_\omega}, \tag{1}$$

where $\varepsilon$ and $\delta_\omega$ are the characteristic wave steepness and relative bandwidth of the frequency spectrum, respectively. For example, if the wave spectrum width is $\sigma_\omega$, $\delta_\omega = \sigma_\omega/\omega_p$, where $\omega_p$ is peak of wave frequency spectrum. Assuming a Gaussian shape of the frequency spectrum, $\delta_\omega$ is equivalent to $1/\sqrt{\pi}Q_p$, where $Q_p$ is the spectrum parameter defined by *Goda* [2000]. Therefore, equation (1) can be simply used given information from wave frequency spectra. The derivation of BFI-kurtosis relates to four-wave interactions as follows. For narrowbanded, unidirectional waves, considering four-wave interactions, kurtosis, $\mu_4$ can be estimated as proportional to the square of *BFI* [*Janssen*, 2003]

$$\mu_4 = \lim_{t\to\infty,\sigma_\omega\to 0} \frac{12}{g^2} m_0^2 \int d\vec{k}_{1,2,3,4} T_{1,2,3,4} \sqrt{\omega_1\omega_2\omega_3\omega_4}\, \delta_{1+2-3-4} R_r(\Delta\omega, t) n_1 n_2 n_3 \tag{2}$$

$$= \frac{\pi}{\sqrt{3}} BFI^2 + 3, \tag{3}$$

where $\vec{k}$ is the wave number, $\omega$ is angular frequency, $m_0$ is the total energy of the wave field, $n$ is the wave action density, $T$ is a kernel function of four-wave nonlinear interactions [*Krasitskii*, 1994], and $R_r$ is the real part of the

[1]Disaster Prevention Research Institute, Kyoto University, Kyoto, Japan.


0148-0227/12/2011JC007788

nonlinear transfer function [*Janssen*, 2003]. The role of skewness in the wave height distribution is less important relative to kurtosis. The skewness usually results from second-order corrections (bound modes) and is weakly affected by the dynamics of free waves [*Onorato et al.*, 2005]. The analytical relationship between kurtosis, the maximum wave height, and the occurrence probability of freak waves has been discussed by *Mori and Janssen* [2006]. For a given nonlinearity of kurtosis, the maximum wave height for weak, nonlinear and narrowbanded spectrum waves follows:

$$P_m(H_{\max}) = 1 - \exp\left\{-N e^{-\frac{H_{\max}^2}{8}}[1 + (\mu_4 - 3)B_H(H_{\max})]\right\}, \quad (4)$$

where $P_m$ is the exceedance probability of maximum wave height, $H_{\max}$. The maximum wave height is normalized by $\eta_{rms}$, $N$ is the number of waves (corresponding to the storm duration), and $A_H$ and $B_H$ are polynomials of $H_{\max}$ [*Mori and Janssen*, 2006]. For $\kappa_{40} = 0$, the results are identical to those following the Rayleigh distribution. If a freak wave is defined as a wave whose height $H_{freak} \geq 2H_s$, integrating the tail of equation (4) we obtain the following simple formula to predict the occurrence probability of a freak wave as a function of $N$ and $\mu_4$:

$$P_{freak} = 1 - \exp\{-e^{-8}N[1 + 8(\mu_4 - 3)]\}. \quad (5)$$

Combining a series of equations, equations (1)–(5), the straight forward expression for freak waves from wave spectra can be obtained analytically.

[4] Recent work on numerical simulations of envelope equations and wave tank experiments have illustrated the influence of directional dispersion on kurtosis evolution in deep water. *Gramstad and Trulsen* [2007] showed a decrease in kurtosis and maximum wave height for directional waves when compared with unidirectional waves based on a series of the modified Nonlinear Schrödinger equation. *Waseda* [2006] and *Onorato et al.* [2009] investigated the monotonic decrease of kurtosis as directional effects become significant. These results showed that directional dispersion effects suppress kurtosis enhancement in directional sea states. Therefore, a more general expression for kurtosis in directional sea states is required. For example, *Mori et al.* [2011] proposed a semiempirical relation as $\mu_4 = f(BFI, \sigma_\theta)$ whereby kurtosis is reduced when directional effects occur, where $\sigma_\theta$ is the directional spread of spectra (directional dispersion)

$$\sigma_\theta = \sqrt{\int d\theta\, \theta^2 D(\theta)}. \quad (6)$$

$D(\theta)$ is the directional distribution. The directional spread defined here can be converted to a Mitsuyasu type $\cos^{2S}\theta/2$ directional distribution analytically using the relation of $\sigma_\theta \simeq \sqrt{2/(1+S)}$. They also discussed the ratio between frequency dispersion and directional dispersion where $R = \sigma_\theta^2/2\sigma_\omega^2$ theoretically represents the relative magnitude of directional dispersion effects. These kinds of directional dispersion effects on kurtosis change were verified by several authors experimentally and numerically [e.g., *Onorato et al.*, 2009].

[5] The discussion about the basic study of freak wave prediction and parameterization has been evaluated mainly under steady conditions, such as those resulting from mechanically generated wave flumes and potential wave theory. More research on freak waves in unsteady conditions is required to understand and validate the theories and mechanisms in realistic weather conditions. There are a few studies analyzing nonlinear focusing conditions of freak wave parameters in the ocean. *Waseda et al.* [2011] showed that narrower directional spreading of the wave spectra was observed in the North Sea. However, it is difficult to generalize the possible weather conditions for freak waves due to the wide variety of weather patterns. Therefore an intermediate study between unsteady conditions and real weather conditions is necessary to understand the possible conditions for freak waves due to nonlinear wave interactions.

[6] Following the above mentioned summary, freak wave occurrence is significantly larger for waves that exhibit steep slopes and narrow frequency and directional bandwidths, but the contributing weather conditions are not clearly understood. The present paper will examine the potential occurrence of freak waves under typhoon conditions as a case study of realistic weather patterns, using a series of numerical simulations with a spectral wave model. The possible conditions when freak waves occur during typhoons will be classified by typhoon regions and discussed in detail. The validation of the numerical experiments with ocean wave data will be discussed briefly.

## 2. Numerical Method

[7] Numerical experiments were conducted with a spectral wave model, the SWAN model [*Booij et al.*, 1999], using a super gradient wind field (denoted SGW hereafter for simplicity) generated by the empirical typhoon model of *Fujii and Mitsuta* [1986]. The SGW gives an empirical wind field of a typhoon as a function of central pressure, characteristic wind radius $r$, and typhoon translation speed $V$. The SGW was used to check the sensitivity of typhoon conditions possibly generating extreme wave characteristics under controlled and relatively realistic conditions. To understand freak wave parameter changes in unsteady weather conditions, the typhoon's central pressure was maintained at a constant value while the characteristic radius and moving speed were allowed to change. Both temporal and spatial wave growth and decay were analyzed to identify characteristics indicative of dangerous freak wave conditions.

[8] The spectral wave model was configured as a linear growth theory for wave energy input, $S_{in}$, and Komen's scheme for wave energy dissipation, $S_{dis}$, was selected with two different nonlinear transfer functions, $S_{nl}$, of the Discrete Interaction Approximation (DIA) [*Hasselmann et al.*, 1985] and modified DIA (MDIA) [*Hashimoto and Kawaguchi*, 2000] to check the sensitivity of nonlinear interactions in the wave field. Overall, the sensitivity of $S_{nl}$ to the target results was not significant in most of the computational domain except during crossing sea states; it will be briefly discussed in section 3. The numerical simulations were performed in a rectangular domain 2000 km by 2000 km with 5 km resolution. The discretization of directional spectra was 72 frequency bins and 36 directional bins.

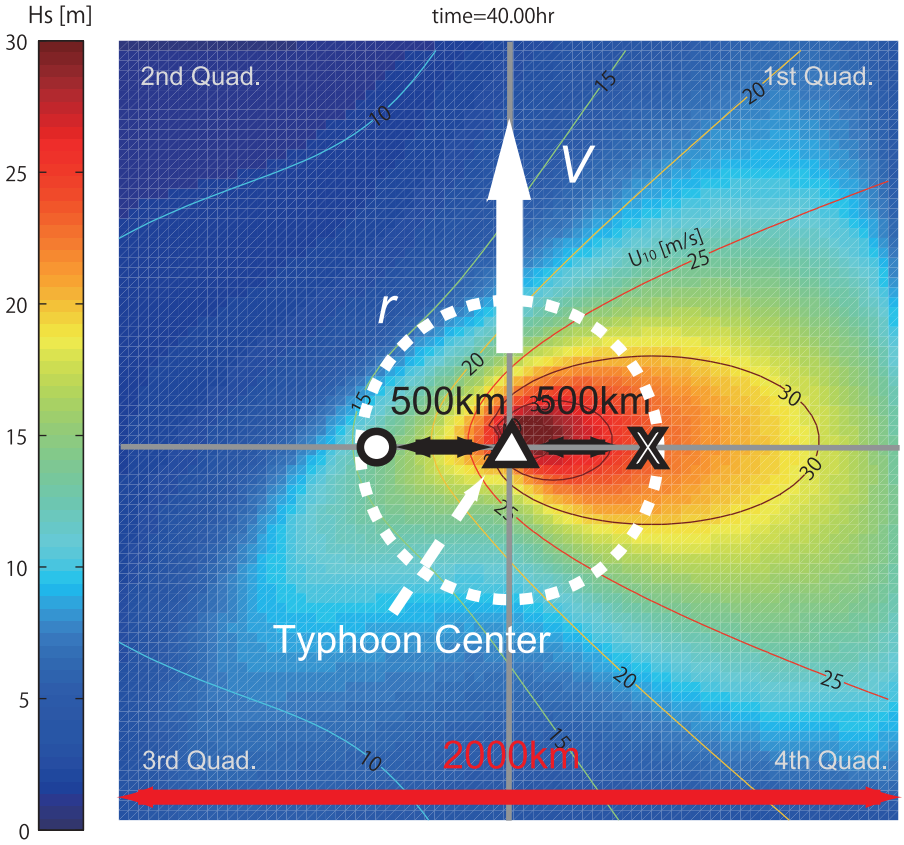


**Figure 1.** Parameters of the empirical typhoon model ($V$, typhoon velocity; $r$, typhoon radius), numerical domain, specific locations for analysis and spatial distribution of $H_s$ (m, colored contours) and $U_{10}$ (m s$^{-1}$, linecontours) for the case of $V$ = 50 km h$^{-1}$ and $r$ = 50 km.

[9] The central pressure was fixed at −60 hPa, while the typhoon speed $V$ ranged from 30 to 50 km h$^{-1}$, and the characteristic wind radius $r$ varied from 50 km to 100 km. Figure 1 illustrates the parameters $V$ and r for the typhoon model. The typhoon moves from south to north, correspondingly from bottom to top in Figure 1. Three marks, an open circle, a triangle, and a cross, indicate the specific locations for the analysis of wave characteristics discussed in section 3. These three locations were selected as a cross section of the typhoon path: 500 km west of the typhoon center, the center itself, and 500 km east of the center. Figure 1 also indicates the spatial distribution $H_s$ (colored contour) and $U_{10}$ (line contour) for the case of $V$ = 50 km h$^{-1}$ and $r$ = 50 km. The SGW gives asymmetric pressure and wind distributions based on observed data, and the results in Figure 1 also indicate asymmetric distributions. A simulated typhoon moves with a constant speed; therefore, the spatial distributions of wave characteristic statistics such as $H_s$, $T_p$, BFI and $\sigma_\theta$ become constant if the coordinates move with typhoon speed $V$.

[10] The analysis of the results focused on the following: (1) spatial distributions of freak wave parameters around the eye of the typhoon and (2) temporal changes of freak wave parameters at different locations relative to the eye. This numerical condition is not exactly realistic, but it will yield information about the general behavior of freak wave parameters and the conditions under which freak waves occur.

## 3. Outline of Field Data

[11] The results of the numerical experiments are compared with field observations. Wave data analyzed here were obtained from the Japanese Nationwide Ocean Wave Information Network for Ports and Harbors (NOWPHAS). The wave data have been collected by ultrasonic wave gauges for 20 min durations every 1–2 h throughout the year. The directional spectra are estimated from surface elevations and two horizontal velocity components of water velocities by the extended maximum entropy method. There are 72 observation stations, and two stations facing the Pacific Ocean at a depth of 50 m were selected for analysis. One station is Hososhima at Miyazaki Prefecture and another is Shionomisaki at Wakayama Prefecture, indicated by a triangle and solid circle on Figure 2. The two stations are located at a similar latitude at a distance of approximately 400 km longitudinally from each other. The typical wave period during typhoons is about 9–10 s; it corresponds to $kh = 2 \sim 3$ which is shallower than the deep water limit. As discussed by *Yuen and Lake* [1982], *Janssen and Onorato* [2007] and *Toffoli et al.* [2009], the shallower effects reduce the instability of nonlinear waves until it becomes neutral at $kh$ = 1.36. However, for the condition of

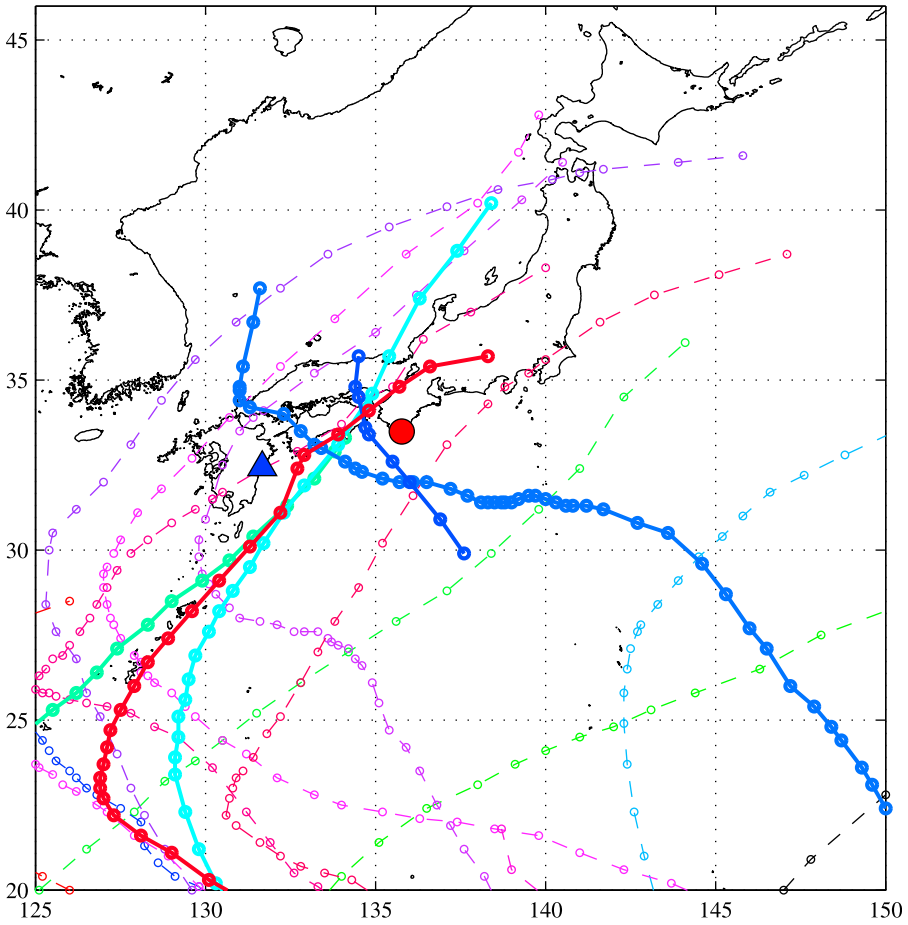


**Figure 2.** Locations of two wave stations and typhoon tracks in 2004 (triangle, Hososhima; solid circle, Shionomisaki; dashed line, typhoon track; solid line, analyzed typhoon tracks).

intermediate water depth, where $kh = 2 \sim 3$, the enhancement of freak wave generation still remains due to four-wave interactions. A total of 19 typhoons approached Japan in 2004, which is double the annual average, and five of these typhoons passed between the two stations as shown on Figure 2. These five typhoons were selected for analysis.

[12] After careful quality checking of the data, the five typhoon data were classified into four categories as east side of typhoon before or after landfall (denoted TC-E-BP and TC-E-AP) and west side of typhoon before or after landfall (denoted TC-W-BP and TC-W-AP). These four categories can be regarded as quadrants around the typhoon eye, spatially, if land effects can be neglected. The time history, wave statistics and both frequency and directional spectra were analyzed, and nondimensional parameters were collected $\pm 24$ h from the closest approach for each typhoon.

## 4. Results and Discussion

### 4.1. Numerical Results

[13] The SGW wind and wave fields were propagated from the south to north end of the computational domain (see Figure 1). The eye of the typhoon passes through the center of the computational domain 40–70 h after the initial condition. At this time the wave field is at a quasi-stationary condition because the fetch is not limited and sufficient time has allowed for wave growth. The spatial distribution of freak wave-related parameters are analyzed at this quasi-stationary time. Temporal and spatial aspects can be interchanged with each other given the constant typhoon speed. Both spatial and temporal characteristics of freak wave related parameters of the typhoon will be discussed in section 4.1.1.

#### 4.1.1. Spatial Distribution

[14] Figure 3 illustrates the spatial distributions of several freak wave parameters and the time series of directional spectra at two locations. The vertical panels in the middle of Figure 3 show spatial distributions of BFI, $H_s$ and $\sigma_\theta$ around the eye for the case of $V = 50$ km h$^{-1}$ and $r = 50$ km. The notation of $t = t_p$ in the figure indicates the time that the typhoon eye is located at the center of computational domain. The eye is located at the center of the figure, and the typhoon moves from south to north (or from the bottom to the top of the figure) with constant speed $V$. The distribution of significant wave height $H_s$ exhibits asymmetry about the center line (north–south) and $H_s$ values east of the eye are larger than those to the west. This asymmetry results from the asymmetric SGW field used as input, resulting from the parameterized asymmetric pressure field and the cyclonic nature of the wind field. As the typhoon translates with a given speed, winds on the east are increased and winds on the west are decreased. The maximum value of $H_s$ is located

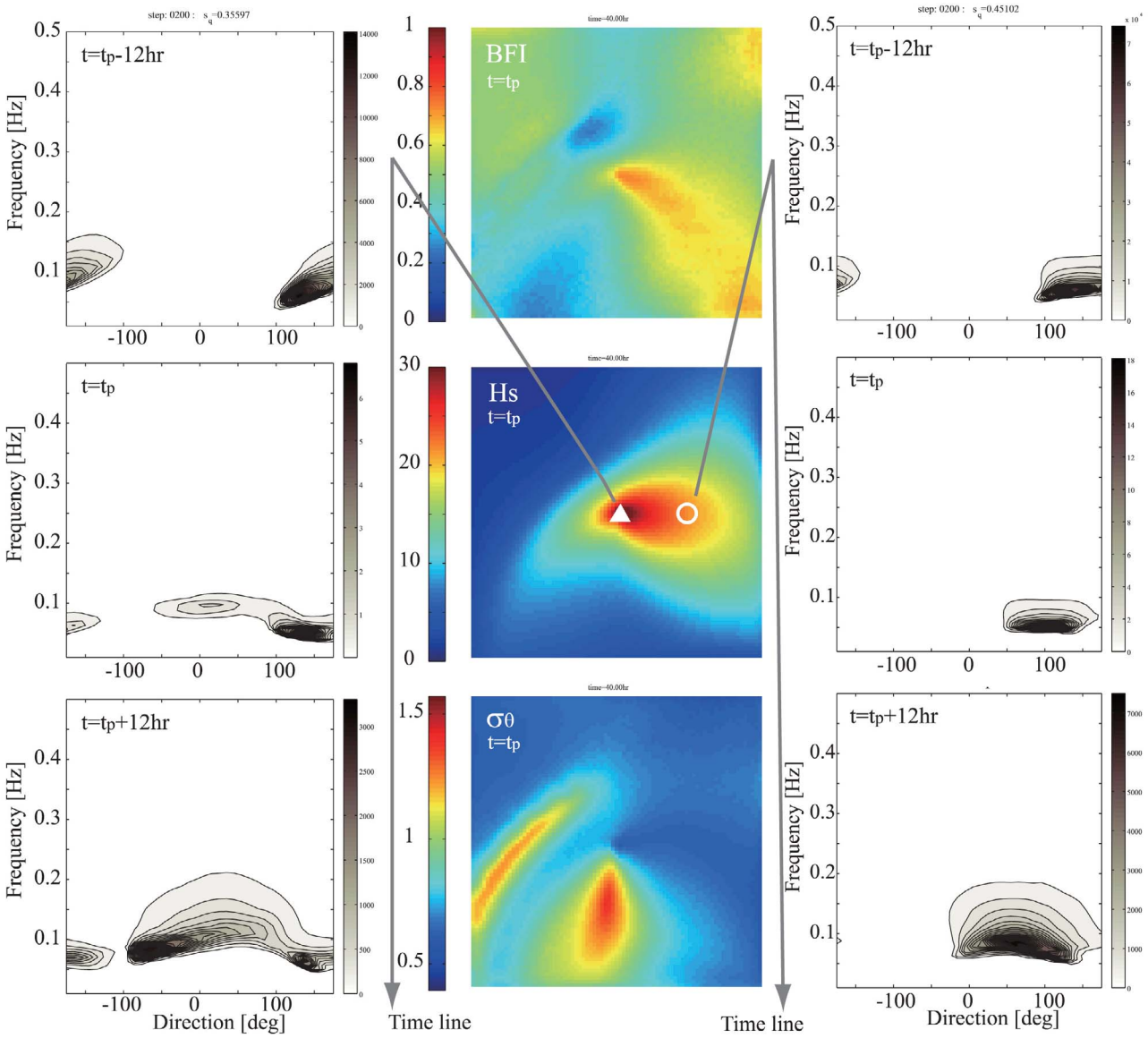


**Figure 3.** Spatial distribution of BFI, $H_s$ and $\sigma_\theta$ around (middle) the typhoon eye and temporal change of directional spectra ((left) eye of the typhoon and (right) +500 km east of the eye, time increases from the top to the bottom of the figure) ($V$ = 50 km h$^{-1}$, $r$ = 50 km).

at the center of the typhoon, and the values decrease rapidly west of the eye. Increased values of $H_s$ continue eastward from the eye.

[15] Previous studies indicate that wave fields with narrow directional spectra, or large values of BFI and small directional spread, are possible conditions for freak waves. Numerical experiments of typhoon waves yield impressive spatial distributions for both BFI and directional spread $\sigma_\theta$. The spatial distribution of BFI is large in the fourth quadrant (relative to the eye). A ridge of elevated BFI values is apparent in the fourth quadrant, extending southeast from the eye with values that exceed 0.6 in that area. However, BFI values in the third quadrant (the southwest) are always less than 0.3. In this quadrant, freak wave occurrence follows linear Rayleigh wave theory under the conditions given by *Mori and Janssen* [2006]. In the fourth quadrant, wave steepness is large, and correspondingly the values of BFI become significantly large.

[16] The spatial distribution of directional spread $\sigma_\theta$ is different from those of $H_s$ and BFI. Directional spread is large both south and west of the typhoon center. Previous studies [*Onorato et al.*, 2009] indicate that large directional spread suppresses the nonlinear enhancement of freak waves as represented by BFI in equation (1). Thus, the wave field in the third quadrant follows linear theory for the prediction of freak waves. And, the wave field in the fourth quadrant, with larger BFI values and narrower directional spread, indicates an area of possible freak wave occurrence given this typhoon condition.

[17] The directional spectra give different points of view of extreme waves. The temporal changes of directional spectra at the eye and along the east side are shown in Figure 3. A single peak in the directional spectra can be

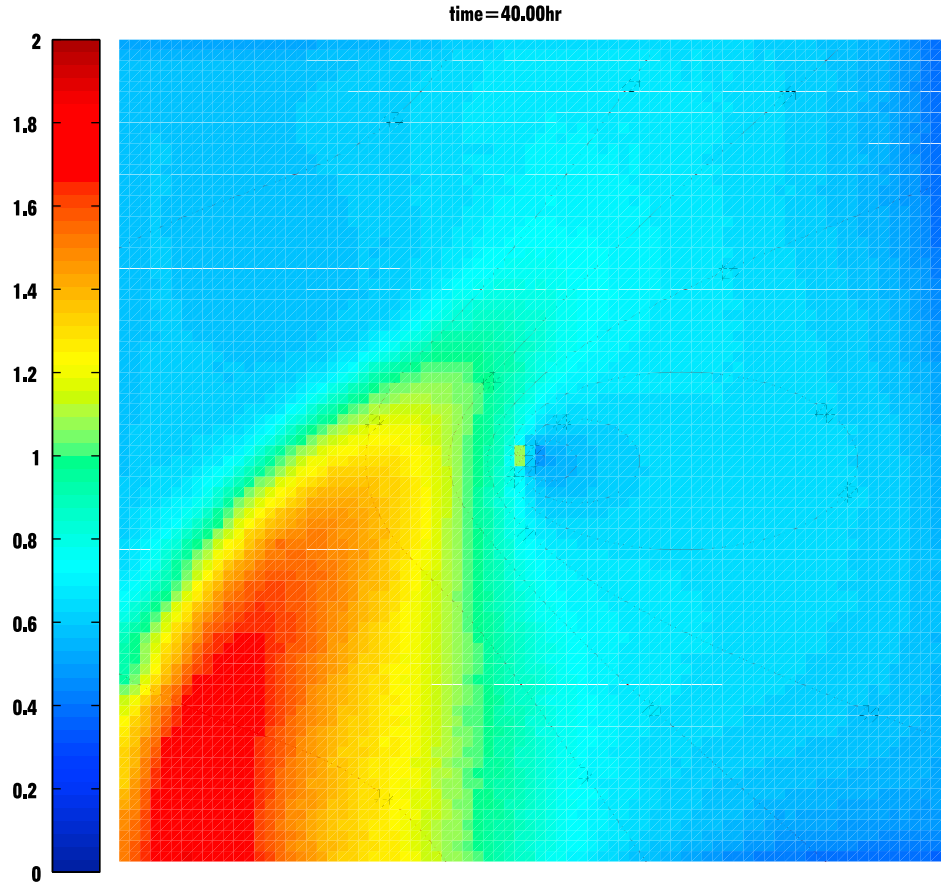


**Figure 4.** Spatial distribution of wave age, $c_p/U_{10}$ (same condition as Figure 3).

observed on the east side but two peaks can be seen at the eye after the closest approach of the typhoon; this explains why directional spread becomes so large in the area south of the typhoon. The qualitative characteristics of directional spectra around the eye agree with field observations of hurricane waves by *Young* [2006]. Although the nonlinear enhancement of freak wave occurrence is weak in bimodal sea states, these bimodal sea states are dangerous, generating crossing/chopping waves. *Tamura et al.* [2009] reported that mixed swell-wind sea states generate narrow spectrum waves. However, the typhoon condition is different because both of the components are young wind waves (wave age in the range of $c_p/U_{10} < 1.5$ as shown in Figure 4). Thus, pure two-wind-wave system crossing can be observed in the area south of the typhoon.

[18] Although a linear crossing sea state can easily generate chopping waves, the role of nonlinear wave interactions on crossing sea states has been discussed during the last decade [*Shukla et al.*, 2006; *Onorato et al.*, 2006; *Toffoli et al.*, 2011]. The particular angle of crossing sea states changes kurtosis values on the scale of $O(\varepsilon^1 T)$. However, a parameterization of nonlinear crossing sea states has not been conducted yet. A more detailed analysis in the area south of the typhoon will be conducted in the near future.

[19] Figure 4 shows the wave age defined by $c_p/U_{10}$, where $c_p$ is the wave celerity of the peak wave number spectra for the same conditions shown in Figure 3. Due to the combination of faster wave speed and lower wind speed, the wave age in the third quadrant (the southwest) is largest and the eastern side of typhoon has the youngest wave age. However, the wave age is still small, therefore, the bimodal sea states in the area south of the typhoon can be regarded as wind waves. Additionally, the spatial distribution of wind and mean wave directions with the directional spread are shown in Figure 5. Both wind and wave directions are within 45° of each other in the first and fourth quadrants. However, the difference becomes more than 90° in the second quadrant. The wind and wave directions are in opposite directions in the third quadrant, and directional spread becomes the largest in this quadrant. The differences in wind and wave directions show good agreement with the spatial pattern of directional spread. This is one reason why directional spread becomes so large in the third quadrant and why two-wind-wave systems exist in this area.

[20] The previous discussion entailed the particular typhoon condition of $V$ = 50 km h$^{-1}$ and $r$ = 50 km. A sensitivity analysis of typhoon velocity and radius was performed, changing the values of $V$ and $r$, respectively. Figure 6 shows the spatial distribution of BFI for different typhoon speeds for the case of $r$ = 50 km. Changing the typhoon radius yields results that are not significantly different, but changing the velocity produces different characteristics in the freak wave parameters. Slower translational speeds produce a concentrated distribution of freak wave parameters around the typhoon eye, while faster speeds yield a more axial, symmetric BFI distribution around the eye.

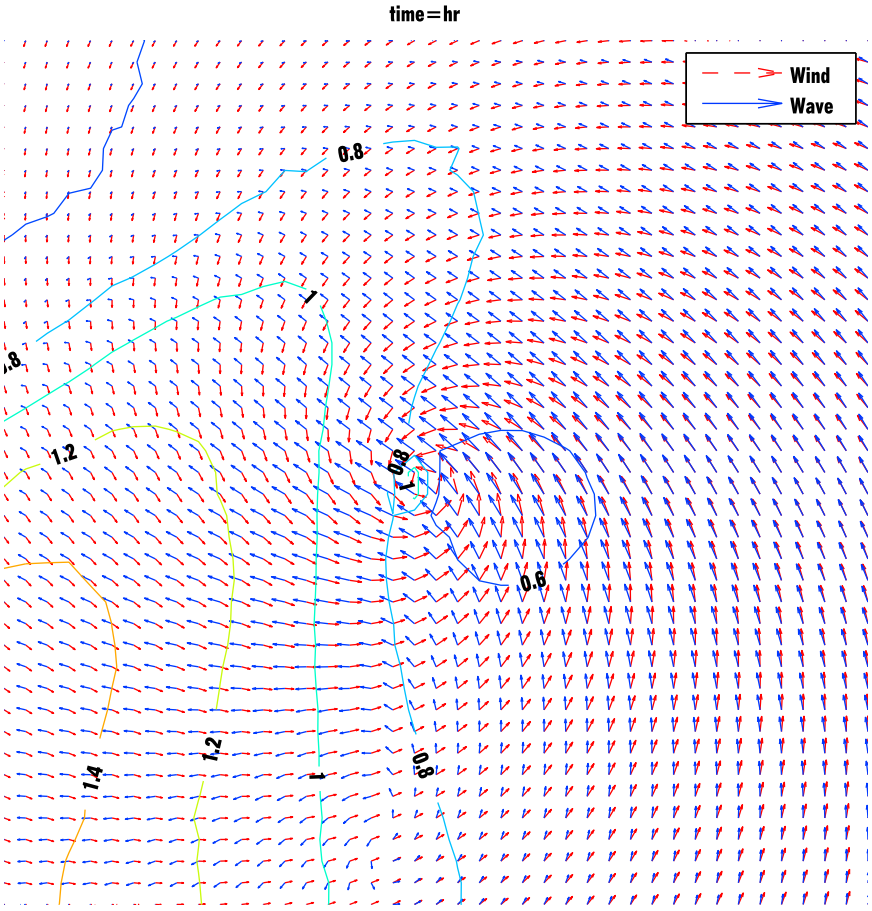


**Figure 5.** Spatial distribution of wind and wave direction (red and blue arrows) and directional spread (contours) (same condition as Figure 3).

Superimposing the wind gradient and translational speed produces this asymmetric result, wherein the faster typhoon ($V = 50$ km h$^{-1}$) has a longer BFI tail in the area southeast of the eye. The spatial distribution of $H_s$ as shown in the middle panel of Figure 3 indicates a peak in $H_s$ in the east–west direction, with a peak in BFI afterward in the fourth quadrant. Although the value of $H_s$ east of the eye is slightly less than that at the peak of the storm, the potential for freak waves occurs later, after $H_s$ peaks in the fourth quadrant. This interesting result is unexpected and warrants further discussion later in this section.

#### 4.1.2. Time Series

[21] Comparing the time series of the freak wave parameters at different locations helps to qualitatively understand the behavior of this phenomena. Figure 7 shows the time series of freak wave related parameters at three different locations for the case of $V = 30$ and 50 km h$^{-1}$ and $r = 50$ km. The time $\tau$ is normalized by $V/r$ and zero indicates the time the typhoon is located at the center of the domain. Changing the typhoon radius generally yields a similar time series with only a difference in duration; therefore, we will focus on changing the typhoon speed and locations.

[22] The history of $H_s$ along a north–south section at the typhoon center indicates rapid growth until the time of closest approach of the typhoon and subsequent decay near the typhoon eye, with relatively mild changes in the surrounding area. As expected, the maximum value of $H_s$ west of the eye is smaller than those calculated at the eye and to the east. The typhoon translation speed changes the maximum value of $H_s$ and the time history east of the eye due to the changing effects of wind speed of the translating typhoon.

[23] At all three locations, BFI started at the same values initially (with very small $H_s$) and exhibited different behaviors afterward as shown in Figure 7b. As observed with $H_s$, BFI values at the typhoon center (along a north–south section) show rapid growth and subsequent decay, although the mechanisms behind the growth and decay are different. BFI relates wave steepness relative to wave frequency bandwidth; the frequency bandwidth becomes broader near the peak of the storm, and after the eye has passed in the area west of the typhoon. On the other hand, for locations east of the eye, BFI reaches a maximum a few hours after $H_s$ reaches a maximum, and the values remain elevated for about a day after the typhoon has passed. This illustrates the main mechanism of how BFI ramps up after the peak of a typhoon. Therefore, potentially dangerous conditions for freak waves due to nonlinear wave interactions remain longer in the area east of the eye. There is no significant dependence of typhoon translation speed on BFI.West of the eye, the values of BFI decrease, remaining below a negligible level (e.g., BFI < 0.4). Additionally, kurtosis exhibits the same behavior, which imparts some physically

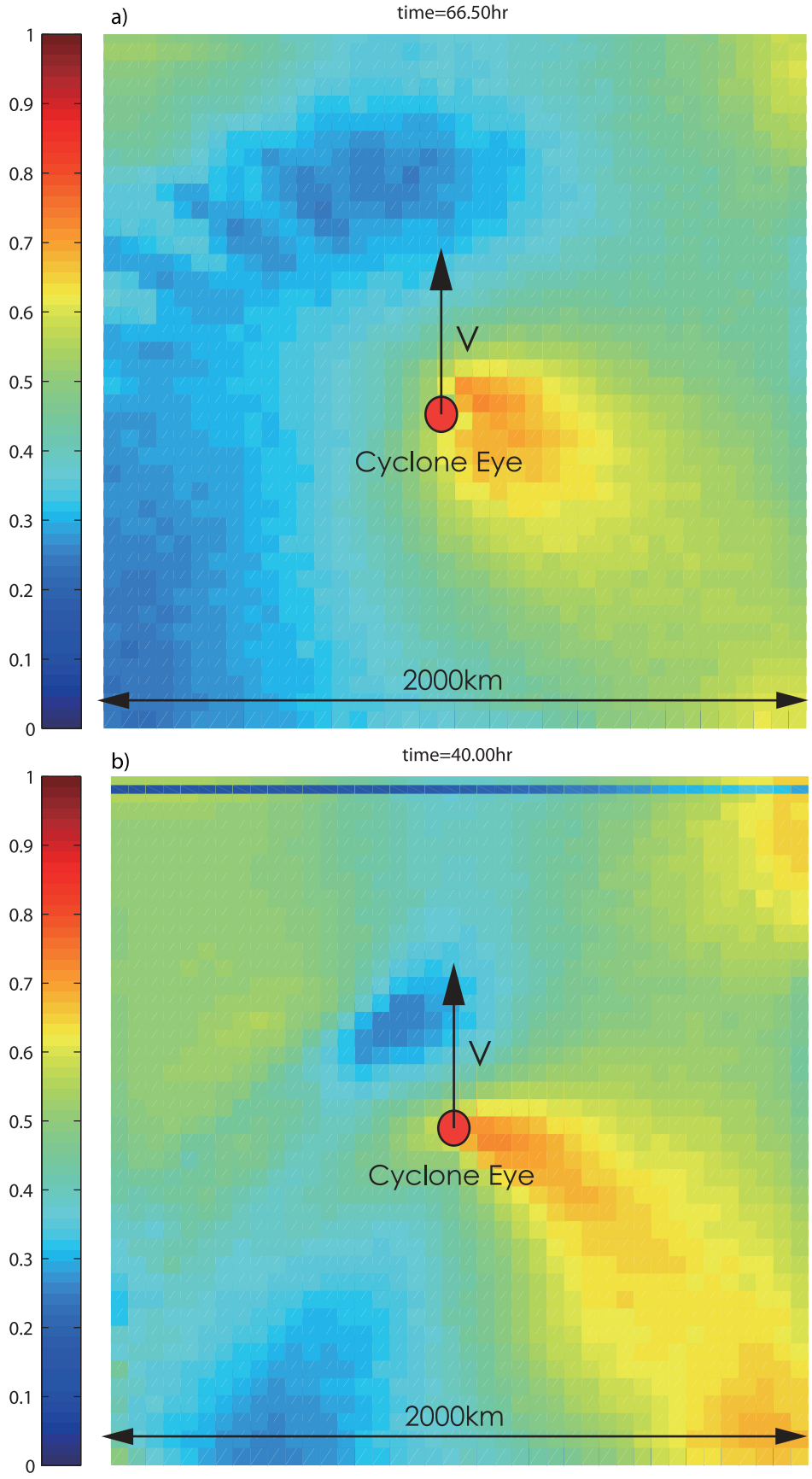


**Figure 6.** Dependence of the spatial distribution of BFI on typhoon speed ($r$ = 50 km; (a) $V$ = 30 and (b) $V$ = 30 km h$^{-1}$).

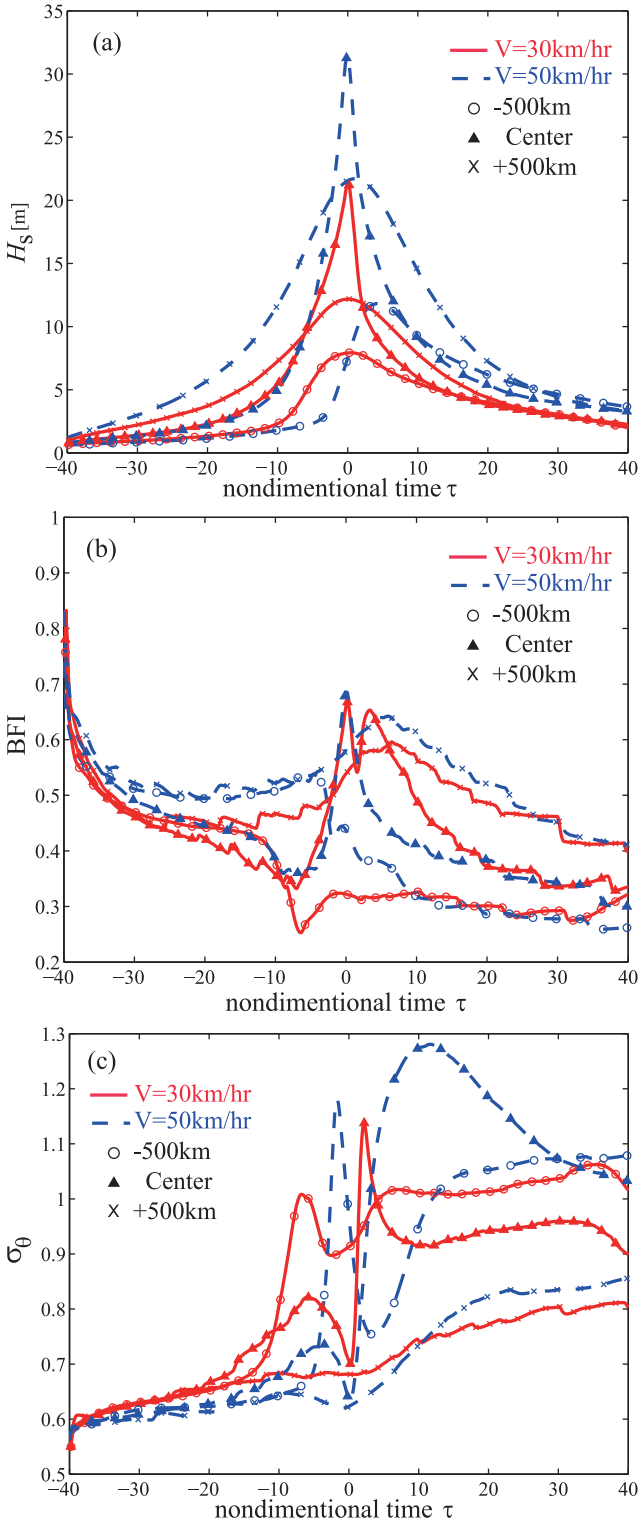


**Figure 7.** (a) $H_s$, (b) BFI and (c) $\sigma_\theta$. Nondimensional time series, $\tau = t \times V/r$, of freak wave related parameters at three different locations (circle, 500 km west; triangle, typhoon center; cross, 500 km east) ($v$ = 30, 50 km h$^{-1}$, $r$ = 50 km).

meaningful information. The kurtosis of surface elevation is a measure of the deviation from the normal distribution, with a value equal to 3 if waves follow a normal distribution. *Mori et al.* [2007] and others investigated whether nonlinear enhancement becomes significant if kurtosis exceeds values of 3.3–3.5. Such large values of kurtosis can only be observed at the typhoon center for short durations, and they continue east of the eye after the typhoon's closest approach. Thus, the nonlinear enhancement of freak waves is basically significant in the area east of the typhoon eye after the closest approach, the same conditions observed with the spatial distribution discussed previously.

[24] Figure 7c shows the time series of directional spread, a parameter that suppresses the nonlinear enhancement of freak wave occurrence. The directional spread, $\sigma_\theta$, is small initially but the values increase after the typhoon's closest approach. At the center, the value of $\sigma_\theta$ fluctuates widely and rapidly increases after the closest approach; this is due to the bimodal spectra as shown in Figure 3. However, east of the eye, the values for directional spread remain relatively small (e.g., $\sigma_\theta < 0.8$). In other words, the fourth quadrant can be regarded as quasi-steady state, similar to an experimental wave flume. However, the third quadrant, in the area south of the eye, exhibits unsteady, bimodal sea states with rapid

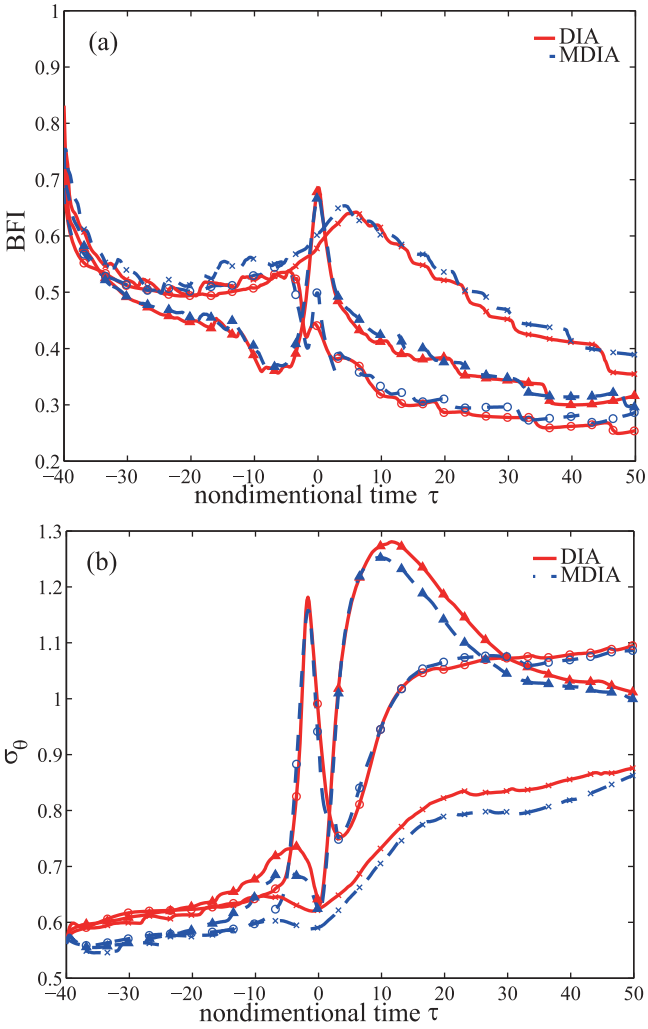


**Figure 8.** (a) BFI and (b) $\sigma_\theta$. Effects of $S_{nl}$ on nondimensional time series, $\tau = t \times V/r$, of freak wave related parameters at three different locations (solid line, DIA; dashed line, MDIA; circle, 500 km west; triangle, typhoon center; cross, 500 km east) ($V$ = 50 km h$^{-1}$, $r$ = 50 km).

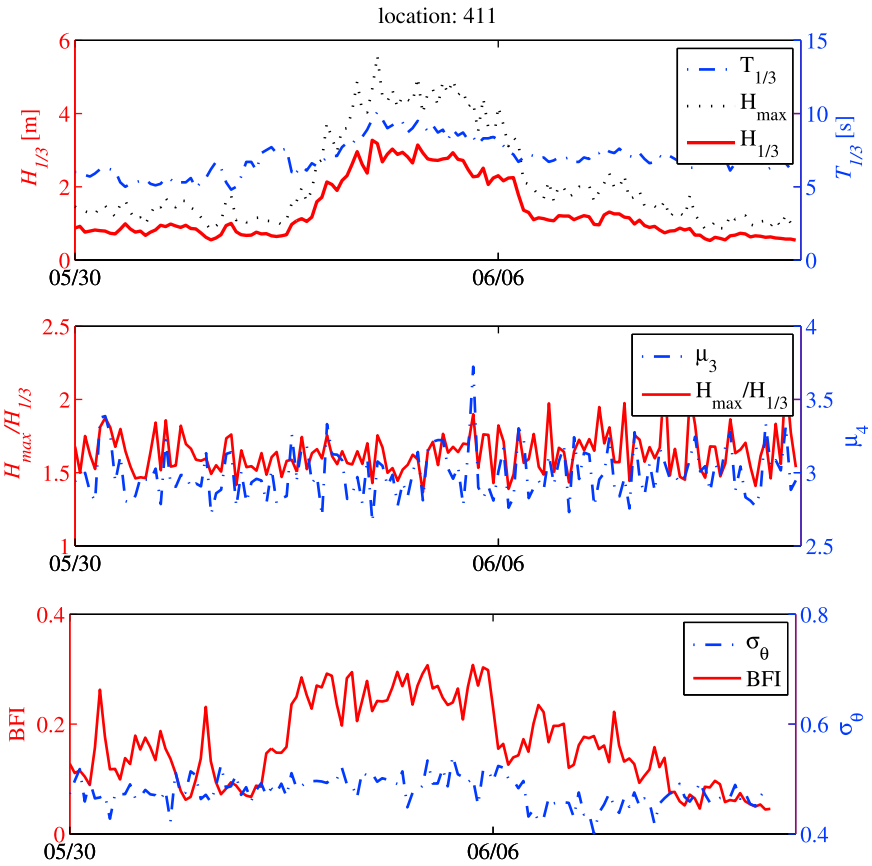


**Figure 9.** Time history of wave statistics for Typhoon Dianmu (T200406) at Hososhima.

changes in wind and wave directions. Lower BFI values and larger directional spread are observed in this area. Although nonlinear effects can be neglected in the third quadrant, the bimodal situation observed here is another important topic to be discussed in future studies.

[25] In the discussion above, the combination of source terms for the wave model was fixed. However, it is expected that the wind input term, $S_{in}$ and nonlinear transfer term, $S_{nl}$, influence the results of wave evolution. A sensitivity analysis of the nonlinear transfer function in the source term was also conducted. Two nonlinear transfer functions, DIA and MDIA, are examined and integrated using the same typhoon condition as discussed before. Figure 8 shows the time series of BFI and $\sigma_\theta$ using DIA and MDIA for the case of $r$ = 50 and $V$ = 50 km s$^{-1}$. Overall, the differences between DIA and MDIA are small except during bimodal sea states. The major differences can be observed in the evolution of $\sigma_\theta$ at the center and west of the eye. The wave field south of the eye becomes bimodal, suggesting that strong nonlinear interactions are occurring. Although the differences between two nonlinear source terms are relatively small, determining the exact nonlinear transfer will be necessary to discuss bimodal sea states quantitatively, and it will be examined in the future.

### 4.2. Analysis of Field Data

[26] Two stations located at a similar latitude facing the Pacific Ocean are picked up for analysis as shown in Figure 2. Five typhoons that passed between the two NOWPHAS stations were selected for analysis. Figure 9 shows the measured data for Typhoon Dianmu (T200406) at Hososhima. Dianmu had a minimum pressure of 915 hPa and the intensity reduced to 965 hPa when it made landfall between the two stations. The time series $H_s$ shows single peaks ranging from 1 to 3.5 m at the height of the storm with a period of $T_{1/3}$ = 10 s. The time series $H_s$ for other typhoons show single peaks ranging from 3–8 m depending on the typhoon intensities and tracks. The conditional sampling of wave statistics for the typhoons was conducted based on the relative locations of the stations and landfall times. The time histories were collected ±24 h from the peak values of moving averaged $H_s$ for each typhoon. Typhoon conditions such as track, central pressure, translation speed and radius differ from each other; therefore, it is difficult to compare the time histories directly. Thus, statistical analysis to calculate the probability density function (pdf) of BFI and directional spread was conducted for the typhoon location (east or west of the eye, and before or after landfall) that corresponds to the quadrants identified in section 4.1.

[27] Figure 10 shows the pdf of BFI, directional spread and $H_{max}/H_{1/3}$ classified by the four categories classified by the four categories described in section 3. Values of BFI on the east sides of the typhoons are larger than on the west sides, and the values continue to become larger after landfall. Overall, BFI reaches the largest values on the east sides after landfall, and the mean BFI on the east side after landfall is 2 times larger than on the west side before landfall. These are consistent with the numerical results shown in Figure 7b.

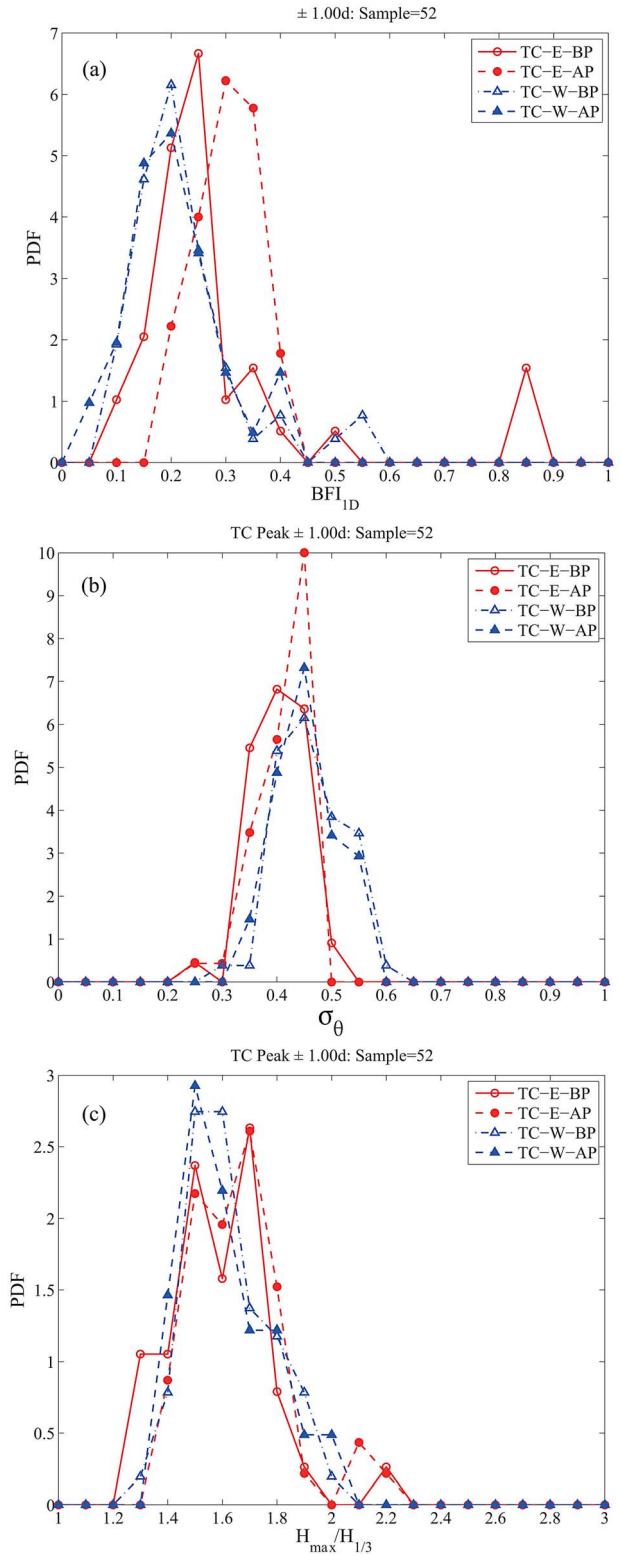


**Figure 10.** (a) BFI, (b) $\sigma_\theta$ and (c) $H_{max}/H_{1/3}$. Pdf of conditional sampled wave statistics of observed data (circle, east station (TC-E); triangle, west station (TC-W); open, before landfall (BP); solid, after landfall (AP)).

On the other hand, there is no significant difference in directional spread before or after landfall. However, the directional spreads are about 30 % different between the east and west stations. This magnitude of difference in directional spread is also expected, as shown in Figure 7c. Regarding the pdf of $H_{max}/H_{1/3}$, the number of observed freak wave conditions ($H_{max}/H_{1/3} > 2$) amounts to three for both sides of the stations. The peak of pdf on the east side is slightly higher than on the west side. However, the total number of samples is only 52 and is insufficient to discuss in detail.

[28] The pdfs of BFI and directional spread show clear increases of BFI and narrower directional spread east of the typhoon after landfall, which is consistent with the numerical experiments. The pdf of maximum wave height normalized by $H_s$, not shown, and kurtosis are statistically not different in comparison with BFI and directional spread. The number of samples is insufficient to discuss statistically sensitive wave parameters such as maximum wave height and kurtosis. Based on the discussion of BFI and directional spread, the potentially higher possibility of freak wave occurrence does not directly reflect the observed extreme wave conditions. Furthermore, it is necessary to consider the influence of land to make quantitative comparisons with coastal buoy data.

## 5. Conclusion

[29] Both numerical experiments and field data analysis of typhoon conditions were conducted to obtain insight into the possible condition of freak wave generation due to nonlinear four-wave interactions. A series of numerical typhoon experiments was conducted using a spectral wave model with an empirical typhoon model and a super gradient wind, while changing the typhoon velocity $V$ and radius $r$.

[30] Summarizing the results, the wave field in the fourth quadrant of the typhoon (southeast of the eye in the Northern hemisphere) exhibits larger BFI values and narrower directional spread. The nonlinear enhancement of maximum wave heights in the fourth quadrant is significantly larger than in the surrounding area. The third quadrant yields an almost linear condition but bimodal spectra can be seen due to the difference in wind and wave directions. The wave field in the fourth quadrant (southeast of the eye) is more prone to freak waves due to nonlinear enhancement, and even though the third quadrant follows a linear condition, it may present a dangerous condition due to bimodal, crossing, sea states.

[31] The results of these numerical experiments were verified by field-observed data. The observed pdfs of BFI and directional spread show clear increases in BFI and narrower directional spread on the east side of the typhoon after landfall; this is consistent with numerical experiments.

[32] Under the assumed typhoon conditions of this study, wave growth yielded a young sea state. The sensitivity of source terms such as wind input and nonlinear transfer will be validated against these results. Furthermore, the influence of the relative speed of group velocity $c_g$ to typhoon translation speed $V$ requires continued discussion since strong energy transfer occurs when $c_g = V$. The hindcasts for real weather conditions, and more fully developed wave conditions, such as those produced by an extratropical storm or a

winter storm at high latitude, should be investigated in the future.

[33] **Acknowledgments.** The author thanks Miguel Onorato and Hajime Mase for their valuable comments on this manuscript. The author appreciates Hiroyasu Kawai from the Port and Airport Research Institute for his support and use of the wave field data. This research was partially supported by the Ministry of Education, Science, Sports and Culture of Japan through a grant-in-aid.

## References

Booij, N., R. Ris, and L. Holthuijsen (1999), A third-generation wave model for coastal regions: 1. Model description and validation, *J. Geophys. Res.*, *104*(C4), 7649–7666.

Dean, R. (1990), Freak waves: A possible explanation, in *Water Wave Kinematics*, edited by A. Tørum and O. Gudmestad, pp. 609–612, Kluwer Acad., Dordrecht, Netherlands.

Dysthe, K., H. Krogstad, and P. Müller (2008), Oceanic rogue waves, *Annu. Rev. Fluid Mech.*, *40*, 287–310.

Fujii, T., and Y. Mitsuta (1986), Simulation of winds in typhoons by a stochastic model, *J. Wind Eng.*, *28*, 1–12.

Goda, Y. (2000), *Random Seas and Design of Maritime Structures*, 2nd ed., World Sci., Singapore.

Gramstad, O., and K. Trulsen (2007), Influence of crest and group length on the occurrence of freak waves, *J. Fluid Mech.*, *582*, 463–472.

Guedes Soares, G., Z. Cherneva, and E. Antao (2003), Characteristics of abnormal waves in North Sea storm sea steas, *Appl. Ocean Res.*, *25*, 337–344.

Guedes Soares, G., Z. Cherneva, and E. Antao (2004), Abnormal waves during hurricane Camille, *J. Geophys. Res.*, *109*, C08008, doi:10.1029/2003JC002244.

Hashimoto, N., and K. Kawaguchi (2000), Extension and modification of discrete interaction approximation (DIA) for computing nonlinear energy transfer of gravity wave spectra, paper presented at 27th International Conference on Coastal Engineering, Am. Soc. of Civ. Eng., Sydney, N. S. W., Australia.

Hasselmann, S., K. Hasselmann, J. Allender, and T. Barnett (1985), Computations and parameterizations of the nonlinear energy transfer in a gravity wave spectrum. Part II: Parameterizations of the nonlinear energy trasfer for application in wave models, *J. Phys. Oceanogr.*, *15*, 1378–1391.

Janssen, P. A. E. M. (2003), Nonlinear four-wave interactions and freak waves, *J. Phys. Oceanogr.*, *33*(4), 863–884.

Janssen, P. A. E. M., and M. Onorato (2007), The intermediate water depth limit of the Zakharov equation and consequences for wave prediction, *J. Phys. Oceanogr.*, *37*(10), 2389–2400.

Kharif, C., E. Pelinovsky, and A. Slunyaev (2008), *Rogue Waves in the Ocean*, 216 pp., Springer, Berlin.

Krasitskii, V. (1994), On reduced equations in the Hamiltonian theory of weakly nonlinear surface waves, *J. Fluid Mech.*, *272*, 1–20.

Lavrenov, I. (1998), The wave energy concentration at the Agulhas current off South Africa, *Nat. Hazard*, *17*, 117–127.

Mori, N., and P. A. E. M. Janssen (2006), On kurtosis and occurrence probability of freak waves, *J. Phys. Oceanogr.*, *36*(7), 1471–1483.

Mori, N., P. Liu, and T. Yasuda (2002), Analysis of freak wave measurements in the Sea of Japan, *Ocean Eng.*, *29*(11), 1399–1414.

Mori, N., M. Onorato, P. A. E. M. Janssen, A. R. Osborne, and M. Serio (2007), Exceedance probability for strongly nonlinear long crested waves, *J. Geophys. Res.*, *112*, C09011, doi:10.1029/2006JC004024.

Mori, N., M. Onorato, and P. A. E. M. Janssen (2011), On the estimation of the kurtosis in directional sea states for freak wave forecasting, *J. Phys. Oceanogr.*, *41*(8), 1484–1497.

Onorato, M., A. Osborne, M. Serio, and S. Bertone (2001), Freak waves in random oceanic sea states, *Phys. Rev. Lett.*, *86*(25), 5831–5834.

Onorato, M., A. Osborne, and M. Serio (2005), On deviations from Guassian statistics for surface gravity waves, in *Rogue Waves: Proceedings Áha Huliköá Hawaiian Winter Workshop, University of Hawaii at Manoa, January 24–28, 2005*, edited by D. Henderson and P. Müller, pp. 79–83, Sch. of Ocean and Earth Sci. and Technol., Honolulu.

Onorato, M., A. Osborne, and M. Serio (2006), Modulational instability in crossing sea states: A possible mechanism for the formation of freak waves, *Phys. Rev. Lett.*, *96*(1), 014503.

Onorato, M., et al. (2009), Statistical properties of directional ocean waves: The role of the modulational instability in the formation of extreme events, *Phys. Rev. Lett.*, *102*(11), 114502.

Osborne, A., M. Onorato, M. Serio, and S. Bertone (2000), The nonlinear dynamics of rogue waves and holes in deep water gravity wave trains, *Phys. Lett. A*, *275*(5–6), 386–393.

Shukla, P., I. Kourakis, B. Eliasson, M. Marklund, and L. Stenflo (2006), Instability and evolution of nonlinearly interacting water waves, *Phys. Rev. Lett.*, *97*(9), 094501.

Tamura, H., T. Waseda, and Y. Miyazawa (2009), Freakish sea state and swell-windsea coupling: Numerical study of the suwa-maru incident, *Geophys. Res. Lett.*, *36*, L01607, doi:10.1029/2008GL036280.

Toffoli, A., M. Benoit, M. Onorato, and E. Bitner-Gregersen (2009), The effect of third-order nonlinearity on statistical properties of random directional waves in finite depth, *Nonlinear Processes Geophys.*, *16*, 131–139.

Toffoli, A., E. Bitner-Gregersen, A. Osborne, M. Serio, J. Monbaliu, and M. Onorato (2011), Extreme waves in random crossing seas: Laboratory experiments and numerical simulations, *Geophys. Res. Lett.*, *38*, L06605, doi:10.1029/2011GL046827.

Trulsen, K., and K. Dysthe (1997), Freak waves—A three-dimensional wave simulation, in *Proceedings of the Twenty-First Symposium on Naval Hydrodynamics*, pp. 550–558, Natl. Acad. of Sci., Washington, D. C.

Waseda, T. (2006), Impact of directionality on the extreme wave occurrence in a discrete random wave system, paper presented at 9th International Workshop on Wave Hindcasting and Forecasting, Environ. Can., Vicotria, B. C., Canada. 2006.

Waseda, T., M. Hallerstig, K. Ozaki, and H. Tomita (2011), Enhanced freak wave occurrence with narrow directional spectrum in the North Sea, *Geophys. Res. Lett.*, *38*, L13605, doi:10.1029/2011GL047779.

Yasuda, T., and N. Mori (1997), Occurrence properties of giant freak waves in sea area around Japan, *J. Waterw., Port, Coastal, Ocean Eng.*, *123*(4), 209–213.

Yasuda, T., N. Mori, and K. Ito (1992), Freak waves in a unidirectional wave train and their kinematics, paper presented at 23rd International Conference Coastal Engineering, Am. Soc. of Civ. Eng., Venice, Italy.

Young, I. (2006), Directional spectra of hurricane wind waves, *J. Geophys. Res.*, *111*, C08020, doi:10.1029/2006JC003540.

Yuen, H., and B. Lake (1982), Nonlinear dynamics of deep-water gravity waves, *Adv. Appl. Mech.*, *22*, 67–327.

N. Mori, Disaster Prevention Research Institute, Kyoto University, Gokasho, Uji, Kyoto 611–0011, Japan. (mori@oceanwave.jp)